P5.6

Spectral Polarimetric Measurements in the Mixed Phase Cloud

J. Verlinde[&], D. Moisseev[*], N. Skaropoulos[*], S. Heijnen[*], F. v.d. Zwan[*] and H. Russchenberg[*]

[&]Department of Meteorology, The Pennsylvania State University
[*]Department of Electrical Engineering, Technical University of Delft
(Corresponding author: J. Verlinde, 502 Walker Building, Pennsylvania State University, University Park, PA 16802. e-mail: verlinde@essc.psu.edu. Phone: (814) 863-9711)

1. Introduction

The detailed processes of mixed phase clouds remains one of the greater challenges to observe remotely. In this study, we used the melting layer in a stratiform precipitation event as a convenient laboratory to test the ability of state-of-the-art polarimetric radars to remotely determine details of the melting process. We present fine spatial resolution radar measurements taken with the Technical University of Delft polarimetric data. We show that these polarimetric measurements can be used to deduce details of the melting process and the scattering properties of the hydrometeors, and hence, such a measurement system can be used to study mixed phase processes.

2. Measurements and analysis methodology

a. Weather conditions

The radar measurements were taken during continuous, widespread rain on 19 September 2001 as part of the BBC campaign at the Royal Dutch Meteorological Institute research site at Cabauw, the Netherlands (http://www.knmi.nl/voorl/nieuws/lanimain.htm).

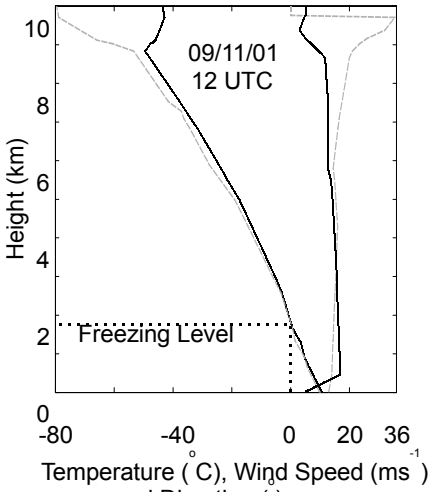

Figure 1: Radiosonde sounding taken at De Bilt 15 minutes after the period of radar observations.

A radiosonde sounding taken at the time of measurements (Figure 1) reveals the thick precipitating cloud layer, extending from 1.7 km to 9 km in height, above a layer of low-level stratus. The freezing level at this time was located at 1850 m, just above cloud base, although radar measurements and other radiosondes indicate that its height fluctuated within a 300 m range, even in the short period of radar measurements (Figure 2). None of A radiosonde sounding taken at the time of measurements (Figure 1) reveals the thick precipitating cloud layer,

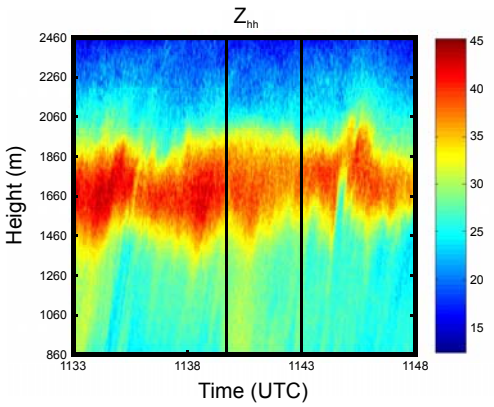

Figure 2: Reflectivty (in dBZ) profiles through the bright band for the 15-minute period of radar observations.

the soundings revealed any indication of an isothermal layers at or just below the freezing level, as is sometimes found in soundings through the bright band (Stewart et al., 1984, Willis and Heymsfield, 1989). Moreover, the wind profile was constant through most of the precipitating cloud layer, with very little change across the melting layer. The speed shear is less than 1 m s^{-1} per km, while the directional shear is negligible in the lower parts of the cloud and only 3° per km in the upper 3 kilometers of the cloud.

b. The radar

The Technical University of Delft Transportable Atmospheric Radar (TARA) provided the bulk of the measurements used in this study (Heijnen et al. 2000). The characteristics of this frequency-modulated continuous-wave (FMCW), three-beam radar are given in Table 1.

Table 1: Characteristics of the TU Delft radar.

Center Frequency	3.3 GHz
Frequency Excursion	2 – 50 MHz
Polarization	XX, YY, XY, YX (linear)
Range	1.5 – 38 km
Range Resolution	3 – 75 m
Sweep Time	1 – 1000 ms
Transmitter Power	140 W
Receiver Noise Figure	1 dB

The main beam allows for polarization diversity, while the two off-axis beams (15° off the main beam in orthogonal directions) are for wind-speed measurements. For this study, time series measurements of the beat signal were recorded for subsequent post-processing. Fifteen minutes of continuous data were analyzed (Figure 2). A frequency excursion of 10 MHz (15 m range resolution), a transmitter attenuation of 20 dB (to avoid receiver saturation), and sweep time of 1 ms were selected for these measurements. The radar was configured in a 5-sweep update cycle: it changed main beam polarization state on a sweep-to-sweep basis (HH, HV, VV) before doing both off-axis beams, resulting in an effective update period of 5 ms for each individual setting (relevant for Doppler processing: Nyquist velocity 4.53 m s^{-1}). The elevation angle was 45°, and the radar looked into the mean cloud-layer wind.

c. Processing

Data for each polarization state was isolated from the full data set, and processed individually. The two off-axis beam data were discarded for this study. A Chebyshev window with 80 dB side-lobe suppression was used for both the range and the Doppler fast Fourier transform (FFT) processing. Doppler processing was done with a 512-point FFT, resulting in a velocity resolution of 3.54 cm s^{-1}. Excessive noise in each spectrum was removed through application of an iterative gradient filter. The 4-minute period demarcated in Figure 2 by the two vertical lines was selected for detailed analysis. The reflectivity profile remained relatively steady during this period. All spectra were unfolded, and shifted by the appropriate amount to place the first moment (mean velocity) of the horizontally polarized spectrum at the zero velocity point. Only data with signal-to-noise ratio (SNR) greater than 10 dB relative the thermal noise spectral floor were retained for further analysis. A mean spectrograph was then constructed for each polarization state by taking the 4-minute mean reflectivity in each velocity bin at all range gates. Mean spectral differential reflectivity ($sZ_{DR}(v) = 10 \log Z_{HH}(v)/Z_{VV}(v)$) and spectral linear depolarization ratio ($sLDR(v) = 10 \log Z_{HV}(v)/Z_{HH}(v)$) were determined by taking ratios of the means in each velocity bin. Spectrographs of the time variability of polarimetric variables (σ^t_{ZDR} and σ^t_{LDR}) were constructed by first calculating the polarimetric spectra for each profile, and then taking the standard deviation in time over each velocity bin at all ranges.

d. The measurements

Current understand is that profiling radar Doppler spectra represent the radar volume hydrometeor fall spectrum convoluted by the radar volume velocity variance spectrum. Both liquid and solid hydrometeors tend to change shape and/or fall characteristics as a function of fall speed, i.e. small, relatively slow falling raindrops are spherical, but become more oblate with increasing diameter (and fall speed), or slow falling ice hydrometeors (dendrites/needles) tend to be oriented horizontally, whereas the faster falling particles are more spherical. As a result, one expects changes in the polarimetric variables as a function of fall velocity. Of course, this will only be the case for a radar-viewing angle where the drop anisotropy affect the measurement.

This is illustrated in Figure 3, with an example of sZ_{DR} in rain. The small, almost spherical particles have Z_{DR} values close to zero (power at horizontal and vertical polarization approximately equal). However, with the increase in oblateness with size, the power in the horizontally polarized returns increase relative to that in the vertical polarization, and the Z_{DR} values increase. Because of the sixth power dependence of the backscatter power to the hydrometeor diameter in the plane of polarization, this increase in Z_{DR} is not linear. The effect of turbulence is to displace individual particles (and hence, their contribution to the total spectral reflectivity) along the velocity axis, such that the contribution of a fast falling oblate hydrometeor in a local updraft eddy in the radar volume may overlay that of a slow falling spherical hydrometeor in a downdraft. Thus, the effect of turbulence is to reduce the curvature in the sZ_{DR} line.

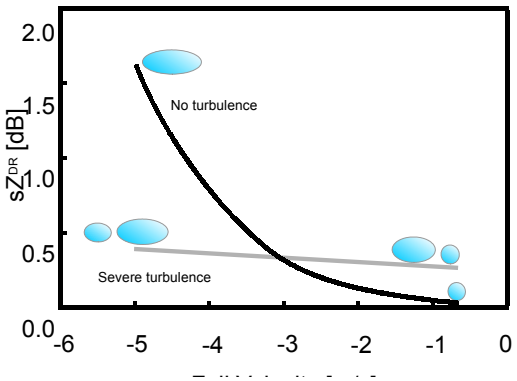

Figure 3: Example of spectral ZDR for cases of no and high turbulence.

LDR is a measure of depolarization of the signal by the hydrometeors, the magnitude of which depends on hydrometeor shape and composition (effective dielectric constant), and orientation relative to the plane of polarization of the incident wave. Because the magnitude of the power in the cross-polar polarization is much less than the co-polar power, the LDR is typically only measurable where mixed-phase

or wetted hydrometeor conditions occur, such as in the bright band.

Both Z_{DR} and LDR depend strongly on the effective dielectric constants (i.e., composition: ice, or ice-air, ice-liquid or liquid), with both measurements decreasing with decreasing dielectric constant. The result may be that highly oriented, dense ice hydrometeors (for example, columns), may have high Z_{DR} and LDR measurements, whereas bigger oriented, but lower density hydrometeors (such as aggregates) may have much lower values.

3. Results

The four-minute averaged spectrographs of co- (Z_{HH}) and cross-polar (Z_{HV}) reflectivity, sZ_{DR}, sLDR, σ^t_{ZDR} and σ^t_{LDR} are shown in Figure 4. Both co- and cross-polar returns were clipped at a 10 dB SNR. Noticeable in the co-polar spectra (Figure 4a) is the spectral leakage at the level of the maximum in the reflectivity. This leakage is the result of a very strong but narrow feature, and could not be removed by windowing. The sZ_{DR} values (Figure 4b) in the leakage peaks are similar to those in the high reflectivity region of each spectrum, distinctly different from the sZ_{DR} values of the surrounding points, making identification of the leakage points easy. The cross-polar power spectra (Figure 4d) are in general much narrower than the co-polar, and are confined to the height limits of higher reflectivity. The first returns above the cut-off SNR detectable are at the height close to where the maximum curvature in the log(Z_e) value is found above the height of the bright band reflectivity maximum. This height is considered to be approximately the level at which melting first starts (Fabry and Zawadski, 1995). Below the maximum in the bright band reflectivity, both co- and cross-polar spectra flare out to cover the full Nyquist interval.

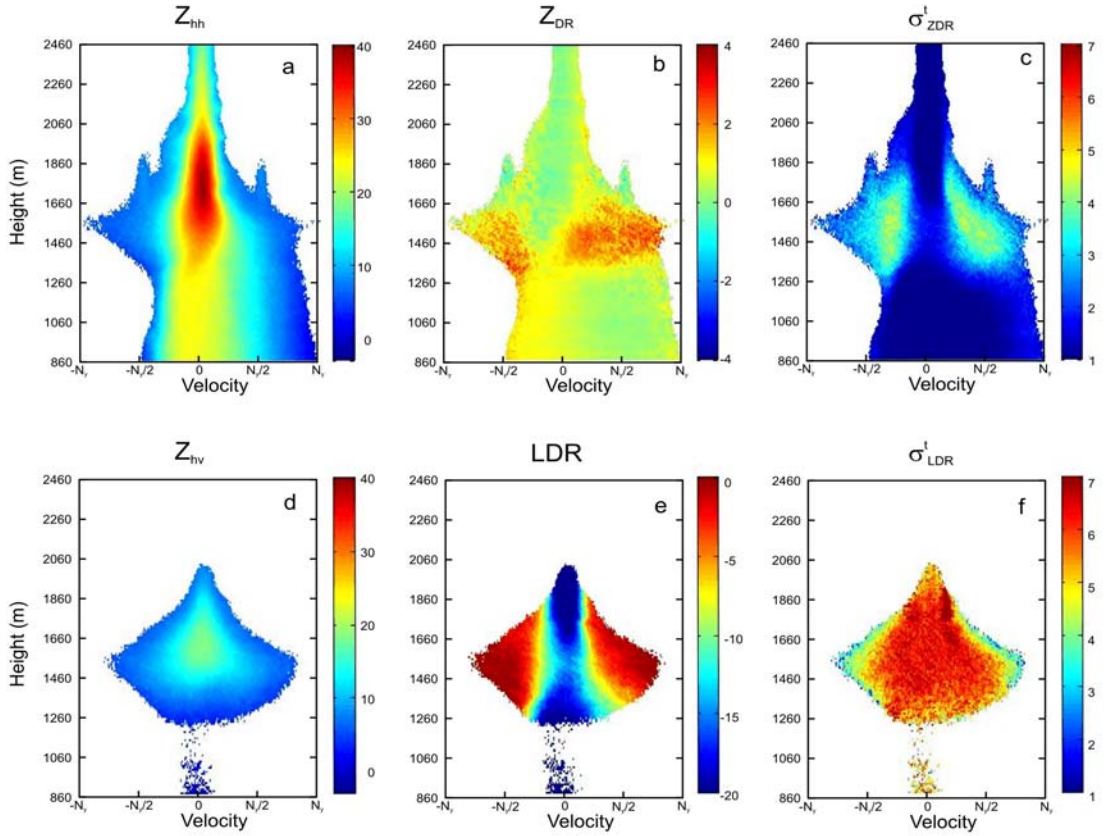

Figure 4: Spectrographs of polarimetric measurements and their variability through the radar bright band.

Looking at the sZ_{DR} panel (Figure 4b), a clear reversal in the slope is discernable going from positive in the snow above the bright band to negative in the rain below. In the snow above, such a slope is suggestive of a population of slow-falling, dense, aligned oblate hydrometeors mixed in with faster-falling, spherical and/or low density ice particles, whereas the slope in the rain below the bright band is as expected (Figure 3). The sLDR spectrograph (Figure 4d) reveals a pattern with a minimum value in the center of the spectrum, increasing towards the edges of the spectrum. The increase in maximum spectral LDR values correlates well with the increase in the width of the cross-polar spectra. The sLDR spectra are almost symmetrical at

heights above the LDR maximum, but become increasingly asymmetric in the below.

The plot of the time variability of sZ_{DR} (σ^t_{ZDR}, Figure 4c) is well correlated with the sLDR plot, suggesting similar causes for the two measurements. The time variability plot in sLDR (σ^t_{LDR}, Figure 4f) reveals peaks in variability on the two edges of the spectrum. These peaks are in the high gradient zone of sLDR, and also follow sZ_{DR} ridges towards the LDR bright band where they then disappear. Another distinctly high region can be found on the left hand side below the LDR bright band, in another region of sLDR gradient and high sZ_{DR}. These regions of high σ^t_{LDR} are in the steep σ^t_{ZDR} slope just to the inside of the regions of high σ^t_{ZDR} values.

4. Discussion

Figure 5 provides greater detail of a few the 4 minute averaged co-polar, sZ_{DR}, and sLDR spectra. The height of each individual spectrum is indicated on the plot of profiles of Z_{hh}, Z_{DR} and LDR. Figure 5a is representative of a spectrum above the melting layer, Figures 5b,c of spectra in the bright band region where the reflectivity increases towards the maximum, Figures 5d,e where the reflectivity decrease below the bright band maximum, and Figures 5f,g below the bright band. Above the bright band the power spectrum is narrow and approximately symmetric. sZ_{DR} has a positive slope through the core of the spectrum, though both edges are characterized by higher sZ_{DR} values. This sZ_{DR} pattern

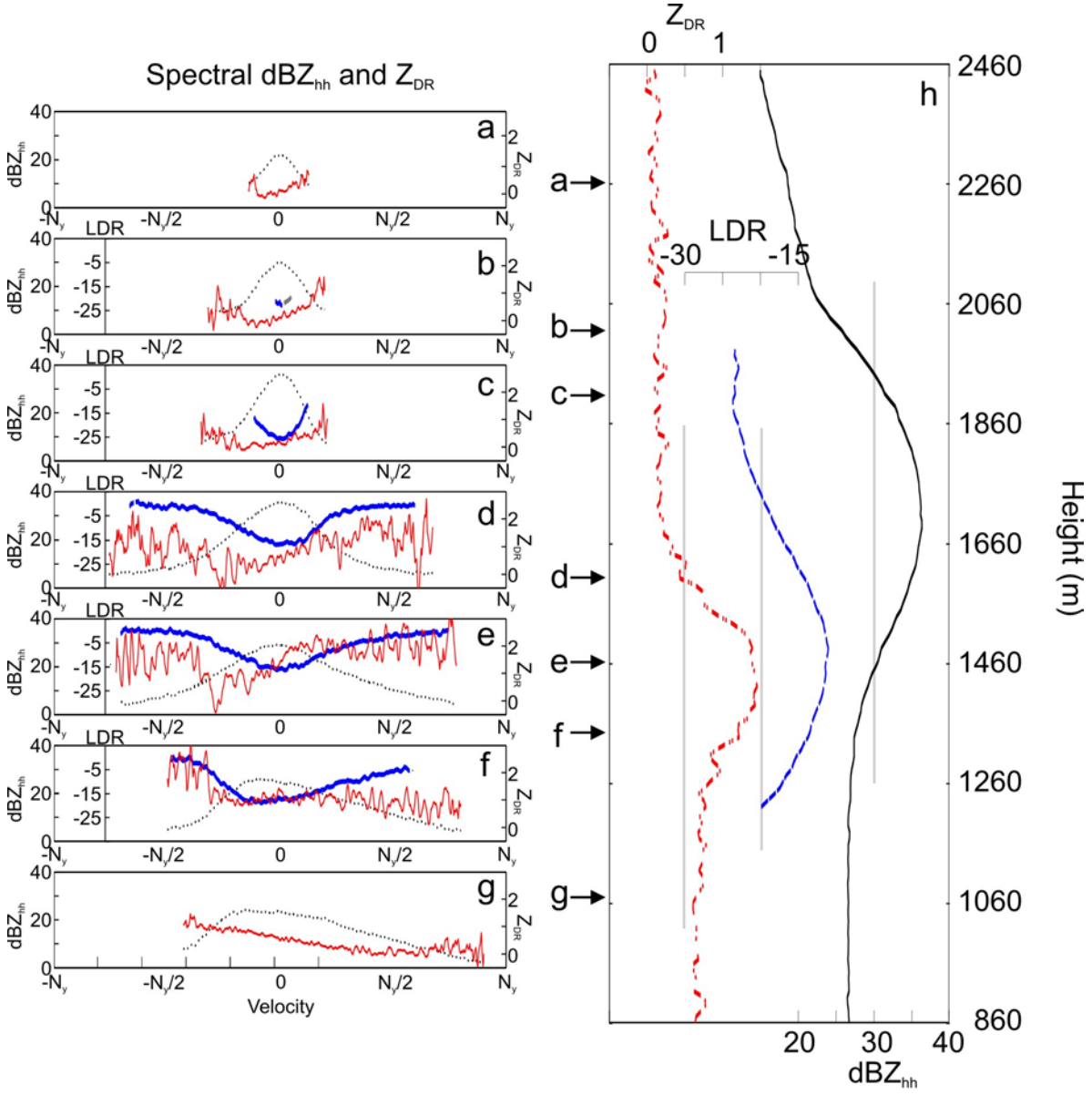

Figure 5: Detailed view of polarimetric spectra evolution with height through the bright band. The black lines represent co-polar reflectivity, red ZDR, and blue LDR.

is consistent with what one would expect from a hydrometeor population consisting out of a relatively small number of slow falling, dense, oriented crystals such as columns or plates (the high sZ_{DR} values at the right edge), a large number of aggregates with decreasing density (and effective dielectric constant) with size (the core of the spectrum), and a small number of more compact aggregates (the higher sZ_{DR} values at the left edge). This picture is also consistent with the Z_{DR} value of approximately 0.2 dB at this height, which is what is expected from a population of aggregates, and with *in situ* observations that indicate that this region is characterized by aggregation (Willis and Heymsfield, 1989).

Melting start at a height of approximately 2000 m as is evidenced from the change in slope of the reflectivity profile (Figure 5h) and the first detectable LDR measurements (Figure 4e). The shape of the power spectrum broadens and changes from symmetric to negatively skewed. The sZ_{DR} slope in the core of the spectrum remains positive, although it flattens somewhat deeper into the bright band. The shoulder in the left edge of the power spectrum is characterized by sZ_{DR} values of approximately 0.5, while the sZ_{DR} values at the right edge have increased to values between 1 and 2 dB. The high SZ_{DR} values at the right edge is what one would expect from an increase in effective dielectric constant with the onset of melting of the high density pristine ice crystals. The left shoulder of the spectrum is consistent with the formation of wet, higher density aggregates formed from the collisions between wet ice crystals/aggregates and/or melting induced compaction. As these higher density aggregates are formed, their contribution to the spectrum shifts towards the faster falling particles, forming the shoulder. From the relative contribution to the total reflectivity it can be deduced that these higher density particles are still relatively few. The observed broadening of the spectrum can be attributed to a broadening of the fall spectrum, since there is nothing in the shear profile nor the actual shape of the power spectrum itself that indicates enhanced turbulence in this layer relative to the layer above. A wider distribution in fall velocities suggests an increase in probability of collision (Fabry and Zawadsky, 1995), since the laboratory results of Mitra et al. (1990) suggest only modest changes in cross-sectional area during the early stages of melting.

The flattening of the sZ_{DR} slope in the core of the spectrum can be brought about in a few different ways. Mitra et al. (1990) found "dry" aggregates to exhibit spinning, helical swing motions as they fall. When melting start, the frequency of rotation and oscillation changed abruptly, both varying within a broad range of values. This behavior continued until the ice structure completely collapsed, at which point the particle suddenly accelerated. The radar-volume averaged shape from a population of spinning, oscillating aggregates will tend to become more spherical than any individual particle, and hence the sZ_{DR} for these particles will tend towards zero. Moreover, if some of the smaller crystals (originally on the right edge of the spectrum) are completely melted into spherical drops, their fall speed will increase somewhat, with the result that their contribution move towards the core of the spectrum, further reducing the sZ_{DR} at those velocity intervals. Thus, in the core of the spectrum, one sees a flattening of the slope.

Considering the details of the aggregate melting process, an alternative explanation can be derived. In the first stage of melting identified by Mitra et al. (1990), small drops of tens of microns in diameter appear at the tips of crystal branches, while the larger crystal structure remains intact. Since the hydrometeor retains the larger aggregate structure, it maintains the aggregate fall characteristics: however, because of the large difference in the dielectric constants for liquid and solid water, it is possible that the individual drops forming at the tips will scatter as individual scatters caught in a coherent structure. That is, the scattering properties are mostly derived from the high dielectric constant droplets. Therefore, the sZ_{DR} values for all the low-density aggregates tend towards that of the drops themselves, with a resulting flattening of the sZ_{DR} slope in the fall velocity range representing these hydrometeors. Of course, the two explanations need not be exclusive, but both can be in effect at the same time.

As melting continues and more low density aggregates compact into higher density, faster falling aggregates, there is a net divergence of scatters, and the integrated reflectivity drops below the height of the bright band maximum. At this time of rapid changes in hydrometeor population, the power spectrum flares out the fill almost the entire Nyquist window (Figure 5d). The power spectrum continues to broaden as particles now fall with a wider range of speeds. The sZ_{DR} values at the edges increase to 1-2 dB and 2 dB at the left and right edges of the spectrum, respectively. The sZ_{DR} transition on the left edge of the spectrum from high positive values to 0 dB occurs rather abruptly (Figure 5e, Figure 4b), while the velocity where the left edge plateaus gradually creeps towards the peak of the spectrum. This results in a rapid increase in the slope of the linear section of the sZ_{DR} spectrum.

The population of hydrometeors is now all at various stages of melting, the exact state of each depending on its original size, shape, and composition. The various small drops of liquid migrate inward from the branch tips and accumulate at the linkages (Mitra et al. 1990), and particles begin collapse into more compact forms even while the melt water acts hold the component crystals together. Thus, the hydrometeors can be expected largely to retain their oblate shapes, and the fall motion to be erratic spinning and oscillating. The flaring out of the spectrum is likely the result of spectral leakage (increase in the spectral noise floor) caused by transient melting effects such as acceleration upon collapsing, rapid particle collapse and/or breakup. Such rapid changes will cause strong fluctuations in the reflected radiation, and also cause

strong depolarization. The LDR peaks in this range. Moreover, the LDR in the wings of the spectrum goes to zero, that is, equal amounts of power in the co- and cross-polar returns, suggesting that the noise floor at both polarizations have been elevated about the thermal noise floor.

The higher leakage induced sZ_{DR} on the right side of the spectrum than the left (Figure 5d) is consistent with a more advanced state of melting (greater mass fraction melted) of the smaller hydrometeors. This continues into Figure 5e, but the change-over point from the linear slope in the core to the flatten part in the right of the spectrum moves towards the maximum in the power spectrum, suggesting that more of the bigger hydrometeors are now sufficiently melted to experience rapid shape changes. As the smaller hydrometeors become mostly melted and collapse completely, there is a reduction in their irregular motions, and the sZDR values at the right hand side of the spectrum lowers (Figure 5f). At the same time, the larger aggregates are now sufficiently melted that they begin to experience rapid changes, and the sZ_{DR}. The result is that the sZ_{DR} spectrum is flat at ~1 dB, except at the extreme left side of the spectrum where the large aggregates are now sufficiently melted that they have high dielectric constants, but at the same time still retain their oblate shapes.

The extension of the melting scattering conceptual model to explain Figure 5d,e,f demands that the scattering from particles of different fall-speeds be different. Bigger aggregates must continue to scatter like individual, but connected drops, while the smaller aggregates scatter more like single, higher dielectric constant (mixture of liquid and ice) oblate particles. Since the spherical melt-drops dominate in the larger melting aggregates, one would again expect low sZ_{DR} values, whereas with the small melting aggregates, the scattering from the ice/water mixture will be sensitive to the shape of the hydrometeor. Hence, sZ_{DR} values of 0 dB are found at velocity ranges where one expect to see large aggregates, and approximately 2 dB at the smaller aggregates. The slope continues to increase throughout the layers where the reflectivity decreases below the bright band as the aggregates continue into stage three melting and the dielectric constant increase (Figure 5h).

At the height where the reflectivity profile straightens out the sZ_{DR} slope becomes flat at a constant sZ_{DR} value of approximately 1 dB when the sZ_{DR} values of the faster falling particles increase (attributed to increases in effective dielectric constant) while that of the slower falling particles decrease (collapse of remaining aggregate ice structure). There is an abrupt change-over to sZ_{DR} values of approximately 3 dB at the faster falling edge, indicative of high dielectric constant, oriented particles, maybe a small number of almost completely melted, big drops, kept intact by what remains of the ice. These high sZ_{DR} values quickly disappear – breakup? – as the slope now reverse to that expected from a population of rain drops (Figure 5g).

5. Conclusions

The observations presented in this paper shows the ability of advanced systems such as TARA to open new areas of research. Although much of the interpretations presented in this paper are highly speculative, it does present hypotheses that can be tested by numerical and or theoretical model. Once hypotheses have be accepted or rejected, at the interpretation of these measurements are on a secure footing, similar measurements can be used to study the variability in melting layer processes and the causes thereof, or alternatively, used to constrain free parameters in modeling studies of melting layer processes.

Acknowledgements: This research has been supported in part by the National Science Foundation under grant ATM 9873643, and by a Marie Curie Fellowship of the European Community Program 'Improving Human Research Potential and the Socio-economic Knowledge Base' under contract number HPMFCT-2000-00679.

References

Fabry, F. and I. Zawadski, 1995: Long-term radar observations of the melting layer of precipitation and their interpretation. *J. Atmos. Sci*., **52**, 838-851.

Heijnen S.H., Ligthart L.P., Russchenberg H.W.J., 2000: First Measurements with TARA: An S-Band Transportable Atmospheric Radar, *Phys. Chem. Earth (B)*, **25**, 995-998.

Mitra, S.K., O. Volhl, M. Ahr and H.R. Pruppacher, 1990: A wind tunnel and theoretical study of the melting behavior of atmospheric ice particles. Part IV: Experiment and theory for snow flakes. *J. Atmos. Sci*., **47**, 584-591.

Stewart, R.E., J.D. Marwitz, J.C. Pace and R.E. Carbone, 1984: Characteristics through the melting layer of stratiform clouds. *J. Atmos. Sci*., **41**, 3227-3237.

Willis, P.T. and A.J. Heymsfield, 1989: Structure of the melting layer in mesoscale convective system stratiform precipitation. *J. Atmos. Sci*., **46**, 2008-2025.